Published by :
http://www.ijert.org

International Journal of Engineering Research & Technology (IJERT)
ISSN: 2278-0181
Vol. 6 Issue 10, October - 2017

Numerical Simulation of Hydromagnetic Convection in a Lid-driven Cavity Containing a Heat Conducting Inclined Elliptical Obstacle with Joule Heating

[+]Dipan Deb, Sajag Poudel, Abhishek Chakrabarti
Department of Aerospace Engineering
Indian Institute of Technology Kanpur
Kanpur, India

***Abstract*— The magnetohydrodynamic convection flow and heat transfer in a lid-driven square cavity is investigated numerically by using the finite volume method. A two-dimensional vertical lid-driven square enclosure with a centrally located heat conducting elliptical obstacle is adopted to simulate the steady, laminar and incompressible flow. Two different sizes of the obstacle are considered with an aim to enhance the heat transfer rate. The governing equations are solved by using the *SIMPLE* algorithm. The left and right vertical walls of the cavity are kept isothermal at two different temperatures whereas both the top and bottom horizontal walls are thermally insulated from the surroundings. Furthermore, a uniform horizontal magnetic field is applied, perpendicular to the translating left lid. The investigations are carried out for a number of governing parameters such as the Hartmann Number 10, Reynolds Number 100, Richardson Number between 1 and 20 Joule heating parameter between 0 and 10 and Prandtl Number 0.71. Two cases of translational lid movement, viz., vertically upwards and downwards are undertaken to study the conjugate heat transport process. The flow and thermal fields are analyzed by means of streamline and isotherm plots.**

Keywords— **magnetohydrodynamic convection, lid-driven square cavity, magnetic field, Joule heating parameter.**

I. INTRODUCTION

Mixed convection flows and heat transfer in lid-driven cavities have widespread scientific and engineering applications such as heat exchangers, cooling of electronic components, industrial float glass production, lubrication and drying technologies, food processing, solar ponds, nuclear reactors, etc.

Prasad and Koseff *(1996)[1]* experimentally investigated the mixed convection within a deep lid-driven cavity of rectangular cross-section and varying depth. Chamkha *(2002)[2]* investigated the unsteady laminar hydromagnetic convection in a vertical lid-driven square cavity with internal heat generation or absorption for both aiding and opposing flow situations. Cheng and Liu *(2010)[3]* elaborated the effects of temperature gradient on the fluid flow and heat transfer for both assisting and opposing buoyancy cases. Billah et al. *(2011)[4]* and Khanafer and Aithal *(2013)[5]* highlighted the role of an obstacle inserted into the cavity as an important enhancer of heat transfer. Later on, Chatterjee et al.*(2013)[6]* and Ray and Chatterjee *(2014)[7]* also studied the effects of an obstacle on the hydromagnetic flow within a lid-driven cavity. Deb, Poudel and Chakrabarti. (2017)[8] studied the hydromagnetic convection in a lid driven cavity containing heat conducting vertical elliptical obstacle with Joule heating. Cheng *(2011)[9]* numerically investigated a lid-driven cavity flow problem over a range of Prandtl Numbers.

Al-Salem et al. *(2012)[12]* studied the effects of the direction of lid movement on the MHD convection in a square cavity with a linearly heated bottom wall. Omari *(2013)[13]* simulated a lid-driven cavity flow problem at moderate Reynolds Numbers for different aspect ratios. Ismael et al. *(2014)[11]* investigated the convection heat transfer in a lid-driven square cavity where the top and bottom walls were translated horizontally in two opposite directions with varying values of partial slip. Khanafer *(2014)[10]* emphasized on the flow and thermal fields in a lid-driven cavity for both flexible as well as modified heated bottom wall.

Hence, motivated by previous works, the present study deals with the numerical simulation of a vertical lid-driven square cavity permeated by a transverse magnetic field and containing a heat conducting solid elliptical obstacle which is inclined at an angle of 45^o to the horizontal centroidal axis.

This template, modified in MS Word 2007 and saved as a "Word 97-2003 Document" for the PC, provides authors with most of the formatting specifications needed for preparing electronic versions of their papers. All standard paper components have been specified for three reasons: (1) ease of use when formatting individual papers, (2) automatic compliance to electronic requirements that facilitate the concurrent or later production of electronic products, and (3) conformity of style throughout a conference proceedings. Margins, column widths, line spacing, and type styles are built-in; examples of the type styles are provided throughout this document and are identified in italic type, within parentheses, following the example. Some components, such as multi-leveled equations, graphics, and tables are not prescribed, although the various table text styles are provided. The formatter will need to create these components, incorporating the applicable criteria that follow.

International Journal of Engineering Research & Technology (IJERT)
ISSN: 2278-0181
Vol. 6 Issue 10, October - 2017

TABLE 1. Nomenclature of various symbols and abbreviations

NOMENCLATURE			
Re	Reynolds Number, $Re=V0Lv$	Rem	Magnetic Reynolds Number
Gr	Grashof Number, $Gr=g\beta(T\ -Tc)L3v2$	T	Dimensional temperature, $[K]$
Ri	Richardson Number, $Ri=GrRe2$	u,v	Dimensional velocity components, $[ms\ ]$
Ha	Hartmann Number, $Ha=B0L\ \sigma\rho v$	U,V	Dimensionless velocity components
Ec	Eckert Number, $Ec=V02cp(T\ -Tc)$	$V0$	Lid velocity, $[ms\ ]$
N	Interaction parameter for MHD, $N=Ha2Re$	x,y	Dimensional Cartesian coordinates, $[m]$
J	Joule heating parameter, $J=N.Ec$	X,Y	Dimensionless Cartesian coordinates
Pr	Prandtl Number, $Pr=v\alpha$	α	Thermal diffusivity, $[m2s\ ]$
Nu	Nusselt Number, $Nu=\ Lkf$	β	Thermal expansion coefficient, $[1K\ ]$
$\theta av\ g$	Average fluid temperature, $\theta avg=\ \theta VdV$	η	Magnetic diffusivity, $[m2s\ ]$
$B0$	Magnetic field strength, $[Wbm2\ ]$	θ	Dimensionless temperature
cp	Specific heat at constant pressure, $[JkgK\ ]$	ρ	Density of the fluid, $[kgm3\ ]$
g	Gravitational acceleration, $[ms2\ ]$	σ	Electrical conductivity, $[1\Omega m\ ]$
kf	Thermal conductivity of fluid, $[WmK\ ]$	v	Kinematic viscosity of the fluid, $[m2s\ ]$
ks	Thermal conductivity of solid, $[WmK\ ]$		
Subscripts			
K	Solid-fluid thermal conductivity ratio	avg	Average
L	Length of the square cavity, $[m]$	c	Cold
p	Dimensional pressure, $[Nm2\ ]$		Hot
P	Dimensionless pressure	f	Fluid
s	Solid		

II. PHYSICAL MODEL

The model describes a two-dimensional lid-driven square enclosure filled with an electrically conducting fluid (Air at Pr=0.71) and having a centrally located heat conducting solid elliptical obstacle inclined at an angle of 450 with the horizontal axis. All the walls are assumed to be impermeable and electrically insulated. The top and bottom horizontal walls are thermally insulated from the surroundings. The left and right vertical walls are kept at temperatures, Tc and T , respectively where $Tc<T$. The left wall is translated vertically upwards as well as downwards in its own plane at a constant velocity $V0$ while all the other walls are kept stationary. A uniform magnetic field $B0$ is applied horizontally, perpendicular to the left lid. The density variation in the buoyancy term is assumed to be taking place according to the Boussinesq hypothesis while all dissipative phenomena except Joule heating are neglected. It must be mentioned here that even though air is not electrically conducting, its use is permissible for numerical simulations. Moreover, a lot of literature is available where air has been used as the working fluid which in turn facilitates numerical validation.

Finally, the magnetic Reynolds Number is assumed to be very small ($Rem=V0L\eta \ll 1$, where η stands for the magnetic

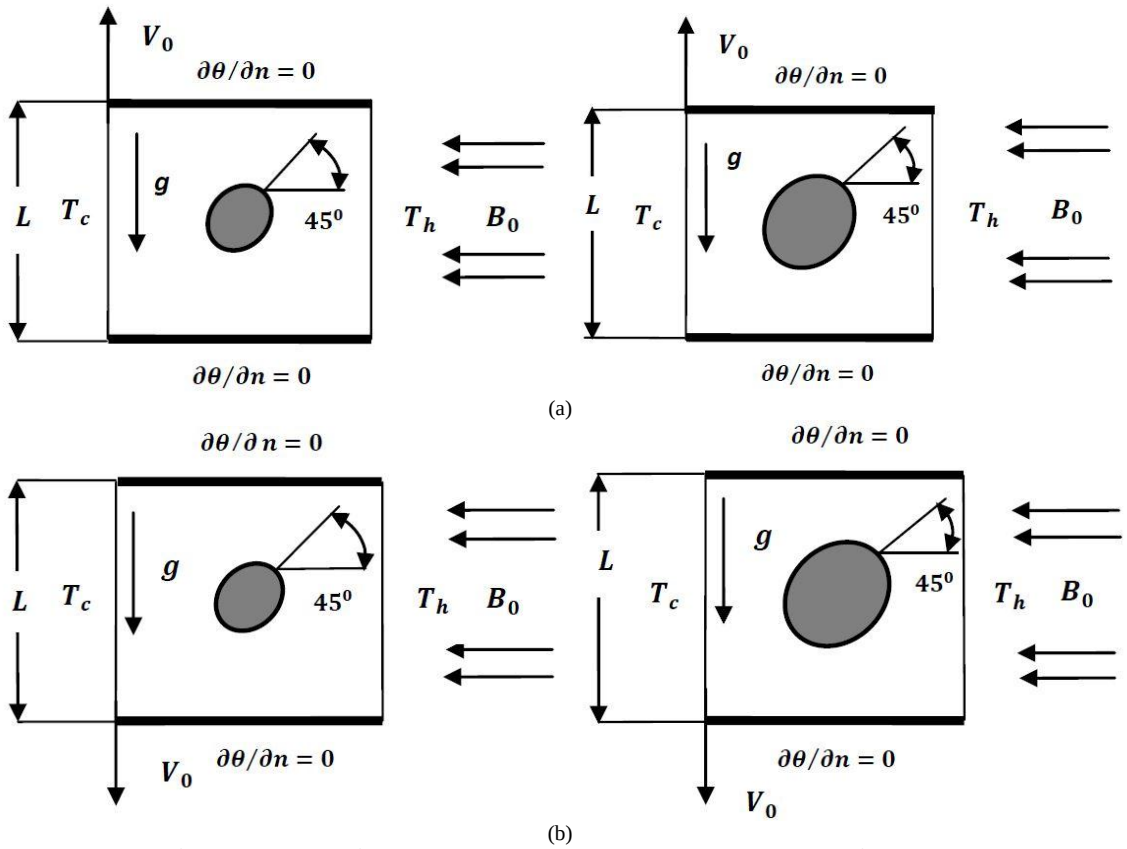

Fig. 1. Schematic representation of the physical model for both obstacle sizes along with the boundary conditions for (a) upward lid motion and (b) downward lid motion

International Journal of Engineering Research & Technology (IJERT)
ISSN: 2278-0181
Vol. 6 Issue 10, October - 2017

diffusivity) so that any induced magnetic field can be safely neglected. A conjugate heat transfer problem involving convective heat transport by the working fluid and conductive thermal transport by the solid obstacle is thus simulated.

III. GOVERNING EQUATIONS

The dimensional forms of the governing equations are as follows:

For the fluid zone:

$$\frac{\partial u}{\partial x}+\frac{\partial v}{\partial y}=0 \quad (1)$$

$$u\frac{\partial u}{\partial x}+v\frac{\partial u}{\partial y}=-\frac{1}{\rho}\frac{\partial p}{\partial x}+\upsilon\left(\frac{\partial^2 u}{\partial x^2}+\frac{\partial^2 u}{\partial y^2}\right) \quad (2)$$

$$u\frac{\partial v}{\partial x}+v\frac{\partial v}{\partial y}=-\frac{1}{\rho}\frac{\partial p}{\partial y}+\upsilon\left(\frac{\partial^2 v}{\partial x^2}+\frac{\partial^2 v}{\partial y^2}\right)-\frac{\sigma {B_o}^2}{\rho}v+g\beta(T-T_c) \quad (3)$$

$$u\frac{\partial T}{\partial x}+v\frac{\partial T}{\partial y}=\alpha\left(\frac{\partial^2 T}{\partial x^2}+\frac{\partial^2 T}{\partial y^2}\right)+\frac{\sigma {B_0}^2}{\rho c_p}v^2 \quad (4)$$

For the solid zone:

$$\frac{\partial^2 T_s}{\partial x^2}+\frac{\partial^2 T_s}{\partial y^2}=0 \quad (5)$$

In order to non-dimensionalize the governing equations, the following non-dimensional parameters are introduced.

$$X=\frac{x}{L},Y=\frac{y}{L},U=\frac{u}{V_o},V=\frac{v}{V_o},P=\frac{p}{\rho {V_o}^2}$$

$$\theta=\frac{T-T_c}{T_h-T_c},\theta_s=\frac{T_s-T_c}{T_h-T_c}$$

The dimensionless governing equations take the following form:

For the fluid:

$$\frac{\partial U}{\partial X}+\frac{\partial V}{\partial Y}=0 \quad (6)$$

$$U\frac{\partial U}{\partial X}+V\frac{\partial U}{\partial Y}=-\frac{\partial P}{\partial X}+\frac{1}{Re}\left(\frac{\partial^2 U}{\partial X^2}+\frac{\partial^2 U}{\partial Y^2}\right) \quad (7)$$

$$U\frac{\partial V}{\partial X}+V\frac{\partial V}{\partial Y}=-\frac{\partial P}{\partial Y}+\frac{1}{Re}\left(\frac{\partial^2 V}{\partial X^2}+\frac{\partial^2 V}{\partial Y^2}\right)-NV+Ri\theta \quad (8)$$

$$U\frac{\partial \theta}{\partial X}+V\frac{\partial \theta}{\partial Y}=\frac{1}{RePr}\left(\frac{\partial^2 \theta}{\partial X^2}+\frac{\partial^2 \theta}{\partial Y^2}\right)+JV^2 \quad (9)$$

For the solid:

$$\frac{\partial^2 \theta_s}{\partial X^2}+\frac{\partial^2 \theta_s}{\partial Y^2}=0 \quad (10)$$

The following dimensionless boundary conditions are implemented:

$U = 0$, $V = 1$ (for upward lid motion), $U = 0$, $V = -1$ (for downward lid motion), $\theta = 0$: at the left vertical wall.

$U = 0$, $V = 0$, $\theta = 1$: at the right vertical wall.

$U = 0$, $V = 0$, $\frac{\partial \theta}{\partial n} = 0$: at the top and bottom horizontal walls.

$U = 0$, $V = 0$: at the surface of the heat conducting solid obstacle.

$(\frac{\partial \theta}{\partial n})_f = K(\frac{\partial \theta}{\partial n})_s$: at the fluid -solid interface.

Here, n is the outward drawn unit normal to a particular solid impermeable wall surface.

IV. NUMERICAL METHODOLOGY

The non-dimensional governing equations along with the aforementioned boundary conditions are solved by using a commercial finite volume-based *CFD* package called *FLUENT*. A pressure-based segregated solver is used and the pressure-velocity coupling is governed by the *SIMPLE* algorithm. The convergence monitors are set as 10−9 for the discretized continuity and momentum equations and 10−12 for the discretized energy equation.

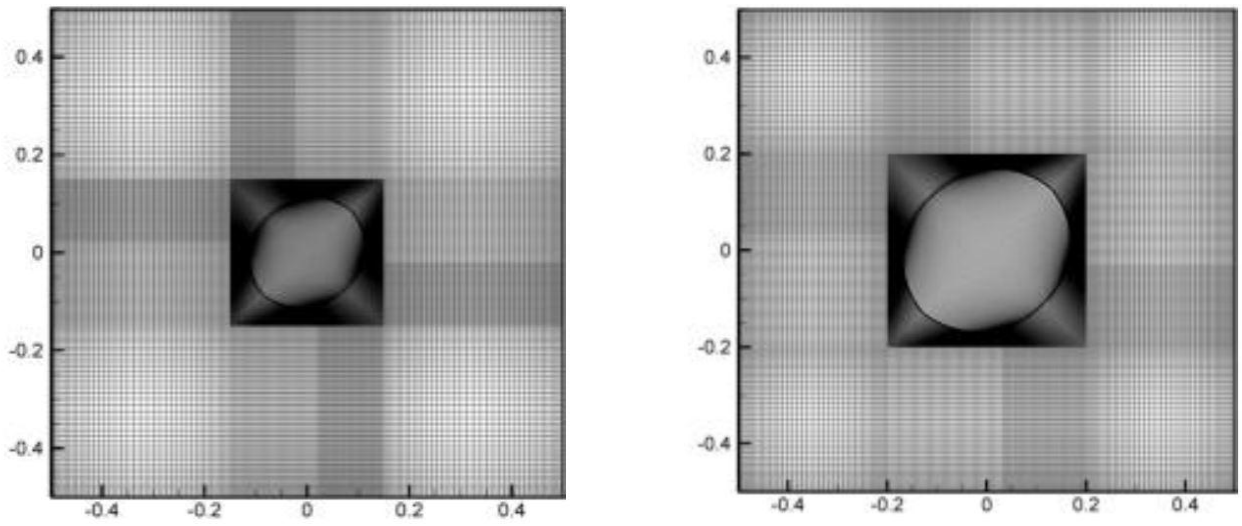

(a) (b)

Fig. 2. Mesh distribution in the computational domain for (a) smaller inclined ellipse and (b) bigger inclined ellipse of surface area 2.25 times the area of the smaller ellipse

International Journal of Engineering Research & Technology (IJERT)
ISSN: 2278-0181
Vol. 6 Issue 10, October - 2017

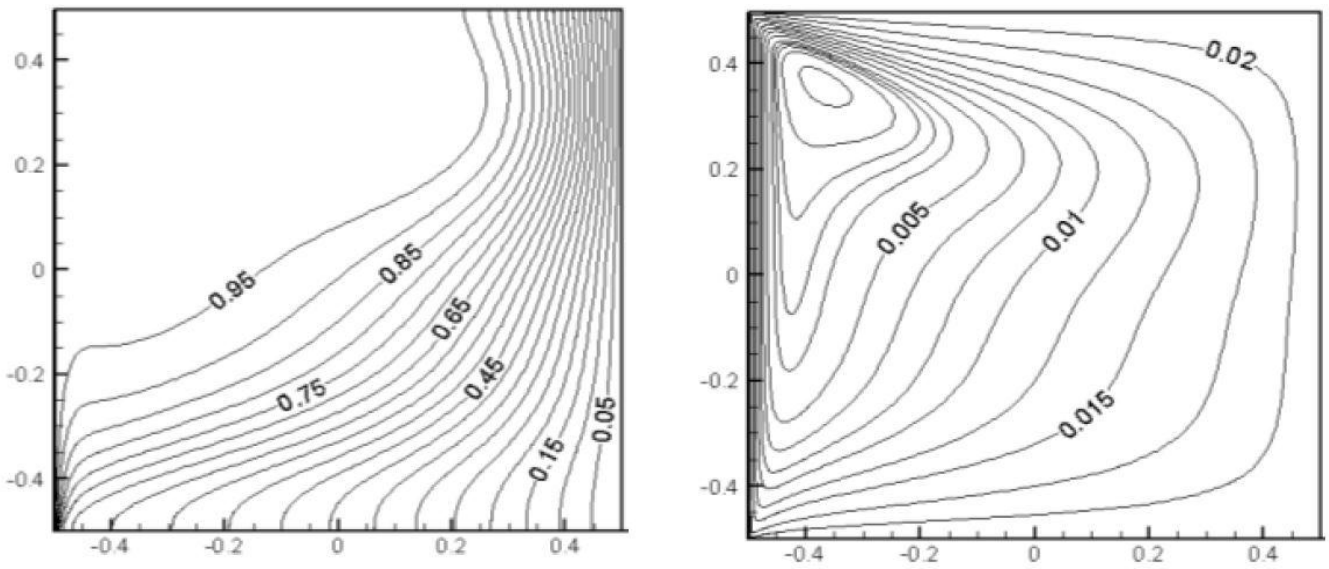

(a) (b)

Fig. 3. Numerical validation with Chamkha (2002) for $\boldsymbol{Re}$=**1000**, $\boldsymbol{Pr}$=**0.71**, $\boldsymbol{Gr}$=**102** and $\boldsymbol{Ha}$=**50**; isotherm on the left and streamline on the right

In order to account for high gradients of the transport quantities in the vicinity of the obstacle and the cavity walls, a non-uniform grid system consisting of a close clustering of grid cells near the rigid cavity walls as well as around the obstacle is adopted for the present computational purpose. Further, in order to assess the accuracy of the results, a comprehensive grid sensitivity analysis has been performed in the computational domain. The following three different mesh sizes were chosen to check the grid independence: ($M1$) 29,396 quadrilateral elements, 29,957 nodes; ($M2$) 38,396 quadrilateral elements, 39,037 nodes; ($M3$) 48,596 quadrilateral elements, 49,317 nodes. Numerical simulations were conducted for Re=100,=0,J=0,Ri=1, and Pr=0.71 for the case of the left wall moving vertically upwards. The simulation data revealed that mesh type ($M2$) is appropriate enough for the present study as a result of which it was selected keeping in mind the accuracy of the numerical results and the computational convenience.

For the purpose of numerical validation, the study made by Chamkha (2002) for the aiding flow situation has been simulated using the present numerical scheme and compared in Figure (3). The qualitative results show good agreement with the reported literature.

V. Results and Discussion

The MHD convection in a vertical lid-driven square cavity is numerically simulated at Re=100, J=1, Ha=10 and $1 \leq Ri \leq 20$. The results are presented in the form of streamline and isotherm contours for both directions of wall movement by taking into account both the obstacle sizes.

Figure (4) highlights the effects of varying Richardson Number (Ri) on the flow field within the lid-driven square enclosure for upward lid motion.

At very low values of Ri, the convection regime evident is of mixed type where both shear and buoyancy forces dominate almost equally on the stream function contours. However, with increase in Ri, the natural convection flow arising out of thermal buoyancy effect starts to predominate. This phenomenon is clearly visible as the counter-clockwise streamlines due to thermal non-homogeneity of the cavity boundaries expand to occupy the major portion of the enclosure, thereby pushing the clockwise streamlines owing to shear-driven flow along the horizontal direction towards the translating left lid. In the vicinity of the left wall, the clockwise eddies gradually shrink in size, elongate along the length of the moving wall and slowly split up into secondary cells having the same sense of rotation. At very high values of the Richardson Number (Ri=20), two more secondary cells appear just adjacent to the solid obstacle on both sides and rotating in the same sense as that of the primary streamlines originating by virtue of thermal buoyancy. However, with increase in the size of the obstacle not much variation is observed in the stream function contours with increasing Ri except those in the immediate vicinity of the obstacle. This is certainly because the streamlines arising out of thermal buoyancy effect in the immediate neighborhood of the obstacle diminish in magnitude despite retaining their overall appearance as they try to conform to the size, shape and orientation of the obstacle.

Figure (5) represents the effect of varying Ri on the streamline contours for the downward translating left wall. The contours depict a completely different scenario as compared to that of Figure (4) as there is only a single recirculating eddy which engulfs the heat conducting obstacle. This is certainly because the downward wall motion causes the aiding flow situation where the shear and buoyancy forces complement each other. The bigger role of recirculating streamlines correspond to the buoyancy-driven convection while the smaller one which is just adjacent to the obstacle

International Journal of Engineering Research & Technology (IJERT)
ISSN: 2278-0181
Vol. 6 Issue 10, October - 2017

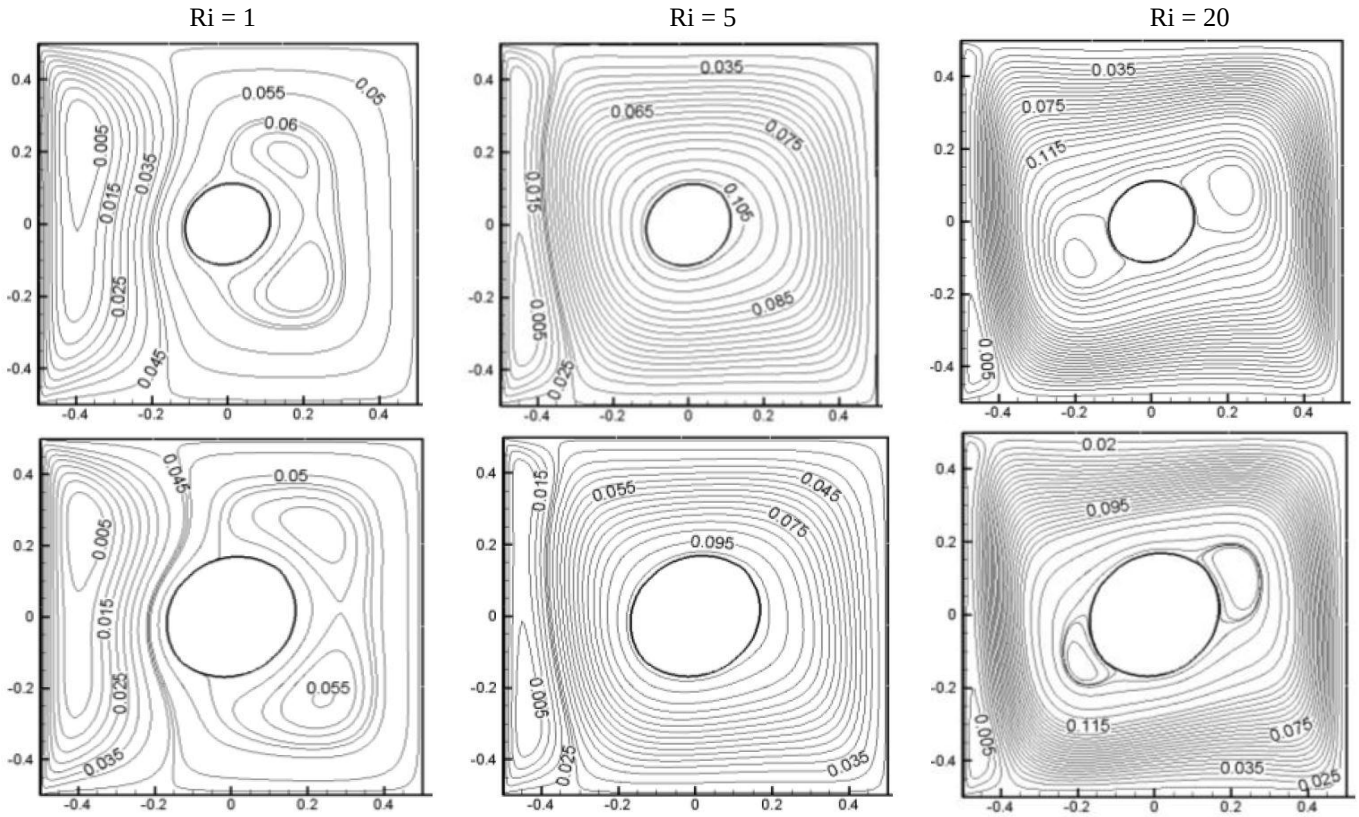

Fig. 4. Effects of ***Ri*** on the streamlines for upward lid motion including both obstacle sizes.

originate from the shearing action of the moving wall. It is seen that with increase in Ri, the streamlines due to shearing effect increase in intensity but decrease in extent. Also, at Ri=20, two secondary eddies develop in the vicinity of the solid obstacle. However, once again it is observed that with increase in obstacle size, the intensities of the streamlines in the immediate vicinity of the obstacle decreases in magnitude.

The isotherms in Figure (6) for upward wall movement exhibit higher gradients with increase in Ri, thus proving that the convection regime shifts towards buoyancy-driven type with rise in the values of the Richardson Number. However, with increase in obstacle size, more isotherms pass through the solid body which indicate an increase in the conduction heat transport mechanism. Qualitatively, there is not much variation in the isotherm patterns for both obstacle sizes except those in the immediate neighbourhood which become more curved with increase in obstacle size to conform to the shape, size and orientation of the obstacle.

Figure (7) shows the isotherms for downward wall motion including both obstacle sizes. The higher gradients as compared to Figure (6) indicate the aiding flow situation in contrast to the opposing flow scenario as depicted by Figure (6). Also, the temperature gradients near the middle of the cavity are higher than those near the cavity boundaries. This indicates that the heat transport process near the stationary right wall follows conduction mode whereas it is via pure natural convection in the middle of the square enclosure except the interior of the solid obstacle where once again the conduction regime predominates. Finally, some forced convection effects are still visible near the translating left wall.

Figure 8(a) depicts the variation of the average Nusselt Number (Nu) on the upward translating left wall with the Joule heating parameter (J) for both the obstacle sizes. It is seen that the average Nu values increase linearly with increasing J for the smaller obstacle size whereas those for the bigger obstacle size initially exhibit a slight increment before falling drastically and then again increase. Also, the curve for the bigger obstacle remains above that for the smaller obstacle. This is because with increase in J, the heat dissipated into the confined fluid medium also increases which aids the overall heat transfer rate. Further, with increase in obstacle size, the backward surge experienced by the clockwise streamlines due to the shearing effect of the upward moving left wall also increases. As a result, the recirculating fluid near

International Journal of Engineering Research & Technology (IJERT)
ISSN: 2278-0181
Vol. 6 Issue 10, October - 2017

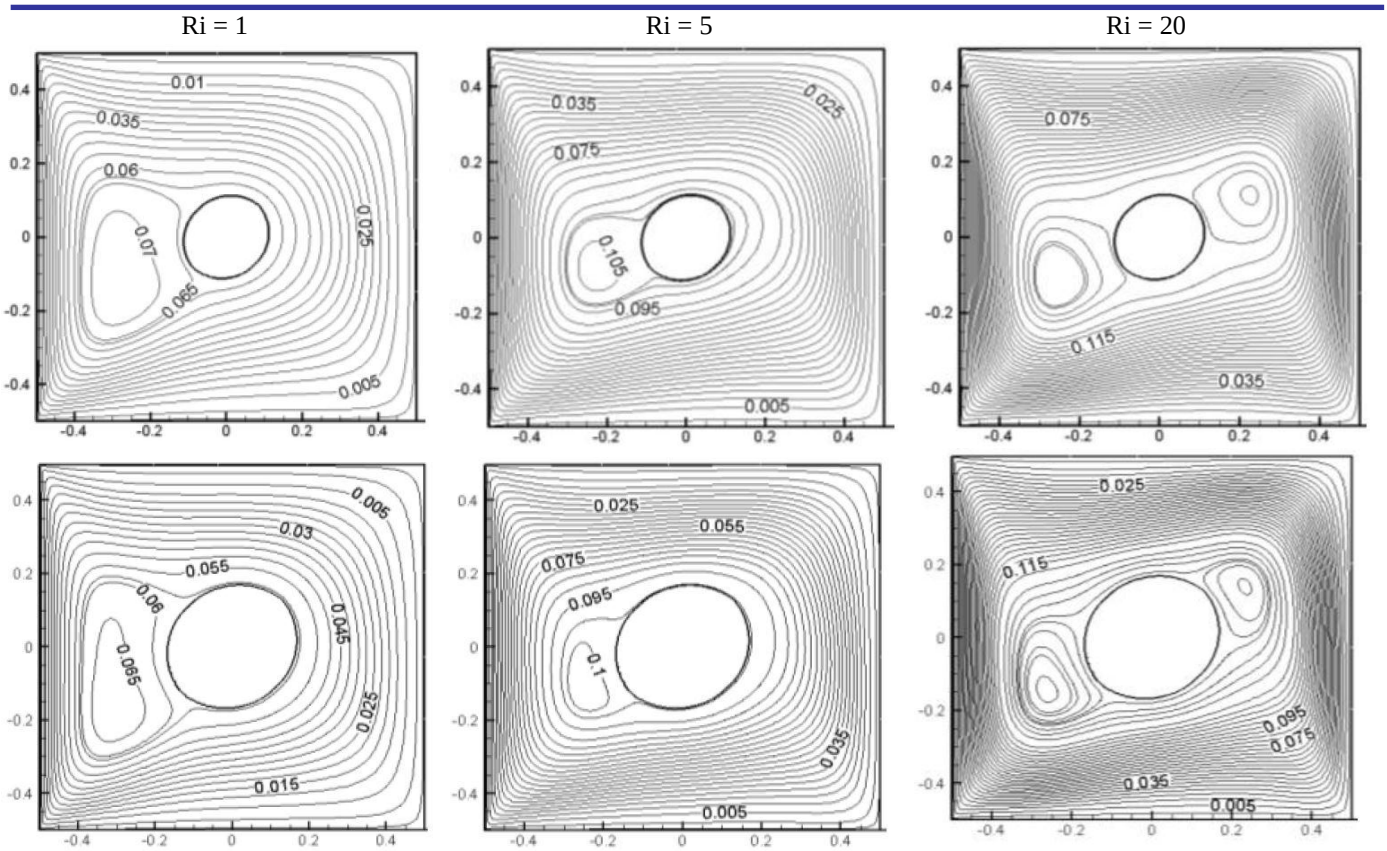

Fig. 5. Effects of ***Ri*** on the streamlines for downward lid motion including both obstacle sizes.

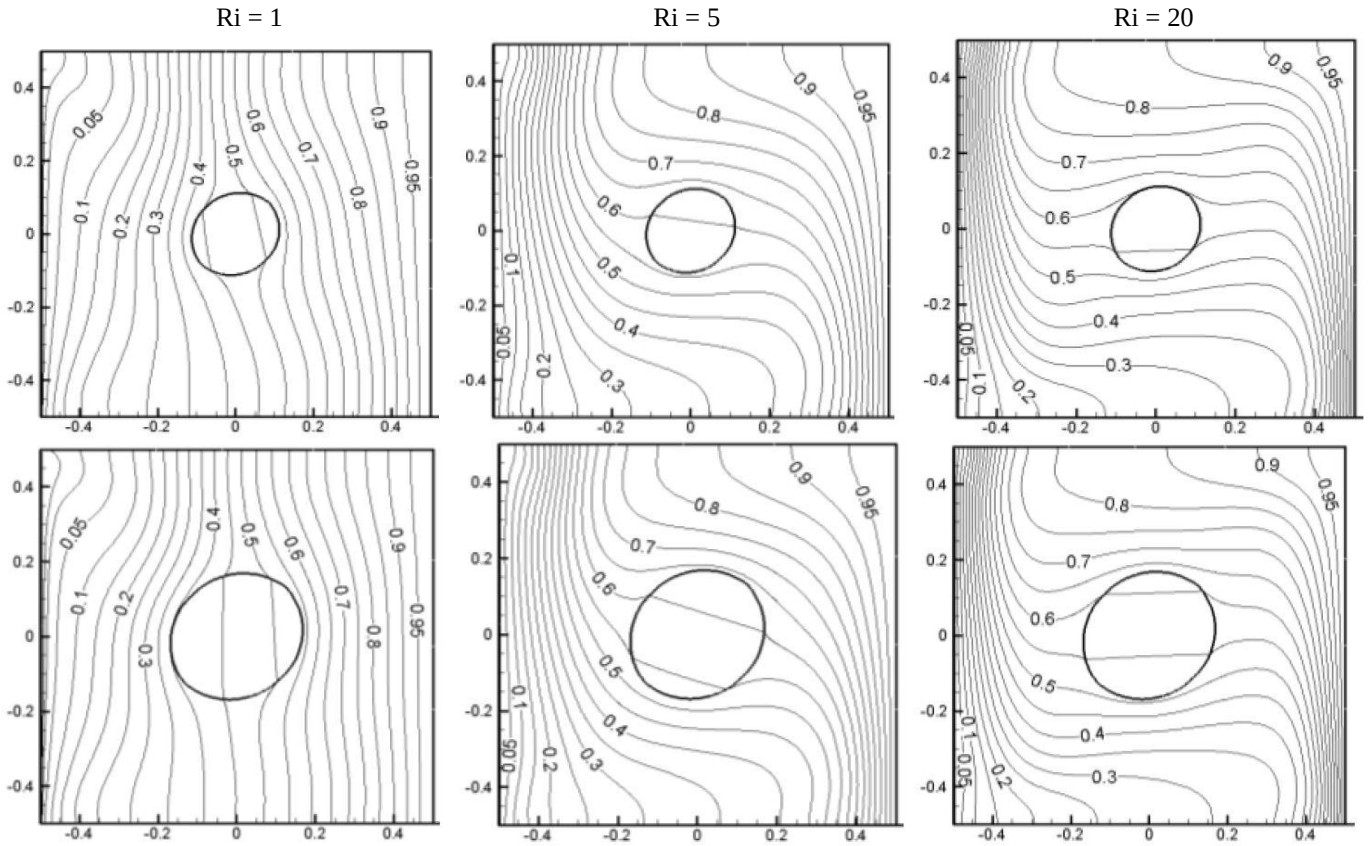

Fig.6. Effects of ***Ri*** on the isotherms for upward lid motion including both obstacle sizes

the left wall impinges more vehemently on it as compared to the case with smaller obstacle dimensions, thereby transferring more heat to the left wall by conduction. These two mechanisms combine to keep the *Nu* values for the bigger obstacle above those for the smaller obstacle.

International Journal of Engineering Research & Technology (IJERT)
ISSN: 2278-0181
Vol. 6 Issue 10, October - 2017

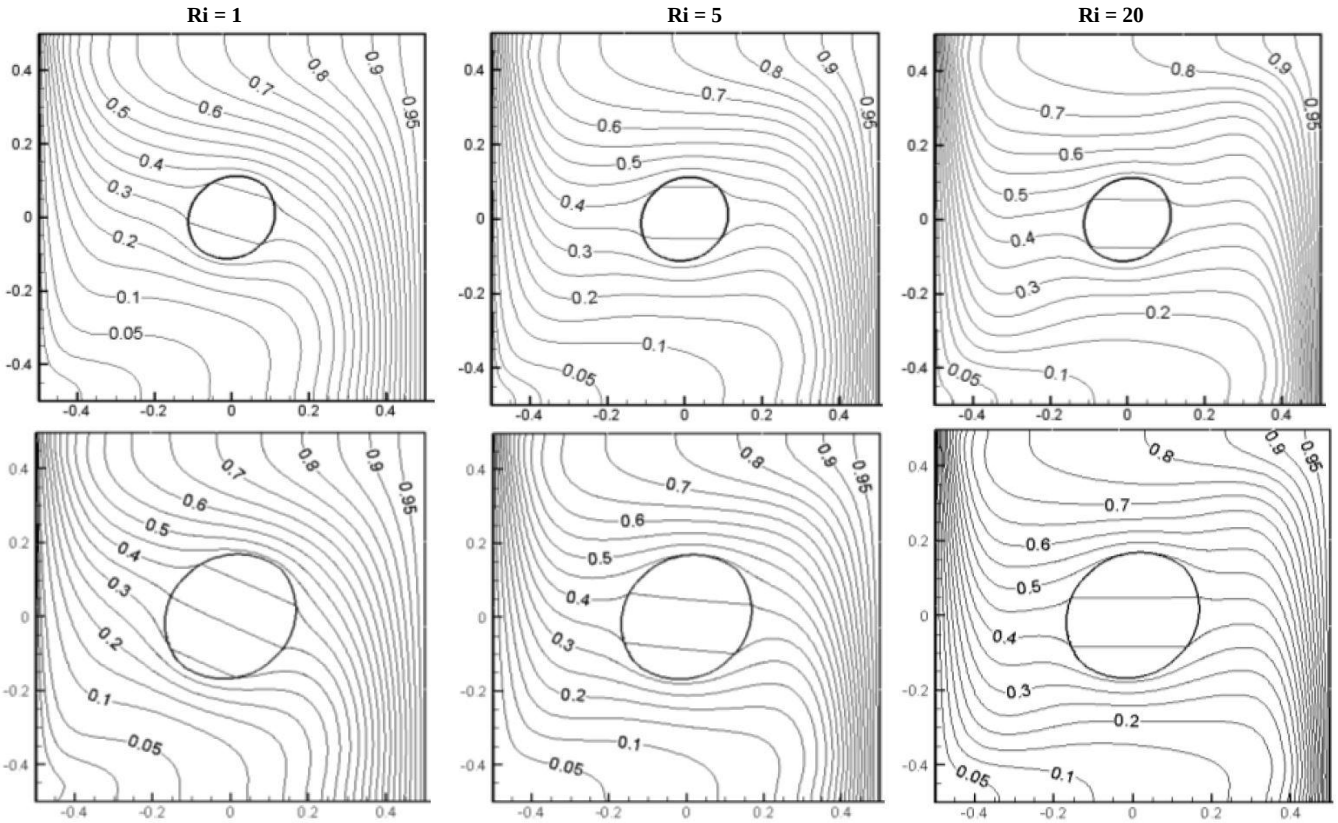

Fig. 7. Effects of ***Ri*** on the isotherms for downward lid motion including both obstacle sizes.

Figure 8(b) exhibits similar variations for downward wall movement. Here also, the variations are almost equivalent to those of Figure 8(a) although the Nu values obtained are comparatively higher as the downward wall motion leads to the aiding flow situation where the forced and natural convection processes reinforce each other, thereby increasing the heat transfer rate. However, the Nu values for the bigger obstacle size gradually fall below those obtained for smaller obstacle dimensions despite being higher initially. This is because with increase in obstacle size, the working fluid gets lesser space to recirculate inside the cavity which leads to lesser convective heat transfer rate as compared to the case with smaller obstacle size.

Figure 8(c) shows the variation of the average fluid temperature, θavg with the Joule heating parameter, J for upward lid motion by taking into account both obstacle sizes. It is seen that θavg increases linearly for smaller obstacle size whereas for the bigger obstacle size, it initially shows slight increment, then falls and again rises. However, the θavg values for smaller obstacle dimensions always stay above that for the bigger obstacle size. This is because, with increase in obstacle size, the space occupied by the fluid medium decreases and that occupied by the solid zone increases which leads to a corresponding fall in the heat transfer rate by the confined working fluid.

Figure 8(d) emphasizes on similar variations for the downward wall motion. The qualitative nature of the curves are similar to those of Figure 8(c) except the fact that the θavg values for the bigger obstacle size are higher than those for smaller obstacle size. This is certainly because the aiding flow situation caused by the downward wall movement seems to nullify the adverse effect of increasing obstacle size on the convection heat transfer process. Moreover, the average fluid temperature values obtained in case of downward wall movement for both obstacle sizes are lower than the corresponding values when the left wall moves vertically upwards.

After the text edit has been completed, the paper is ready for the template. Duplicate the template file by using the Save As command, and use the naming convention prescribed by your conference for the name of your paper. In this newly created file, highlight all of the contents and import your prepared text file. You are now ready to style your paper; use the scroll down window on the left of the MS Word Formatting toolbar.

VI. CONCLUSIONS

The MHD convection flow in a vertical lid-driven square cavity has been simulated for both directions of wall movement and including both obstacle sizes. It is seen that an increase in Ri causes a subsequent increase in the natural convection phenomenon. The upward lid motion causes an opposing flow situation whereas the downward lid motion leads to the aiding flow scenario.

International Journal of Engineering Research & Technology (IJERT)
ISSN: 2278-0181
Vol. 6 Issue 10, October - 2017

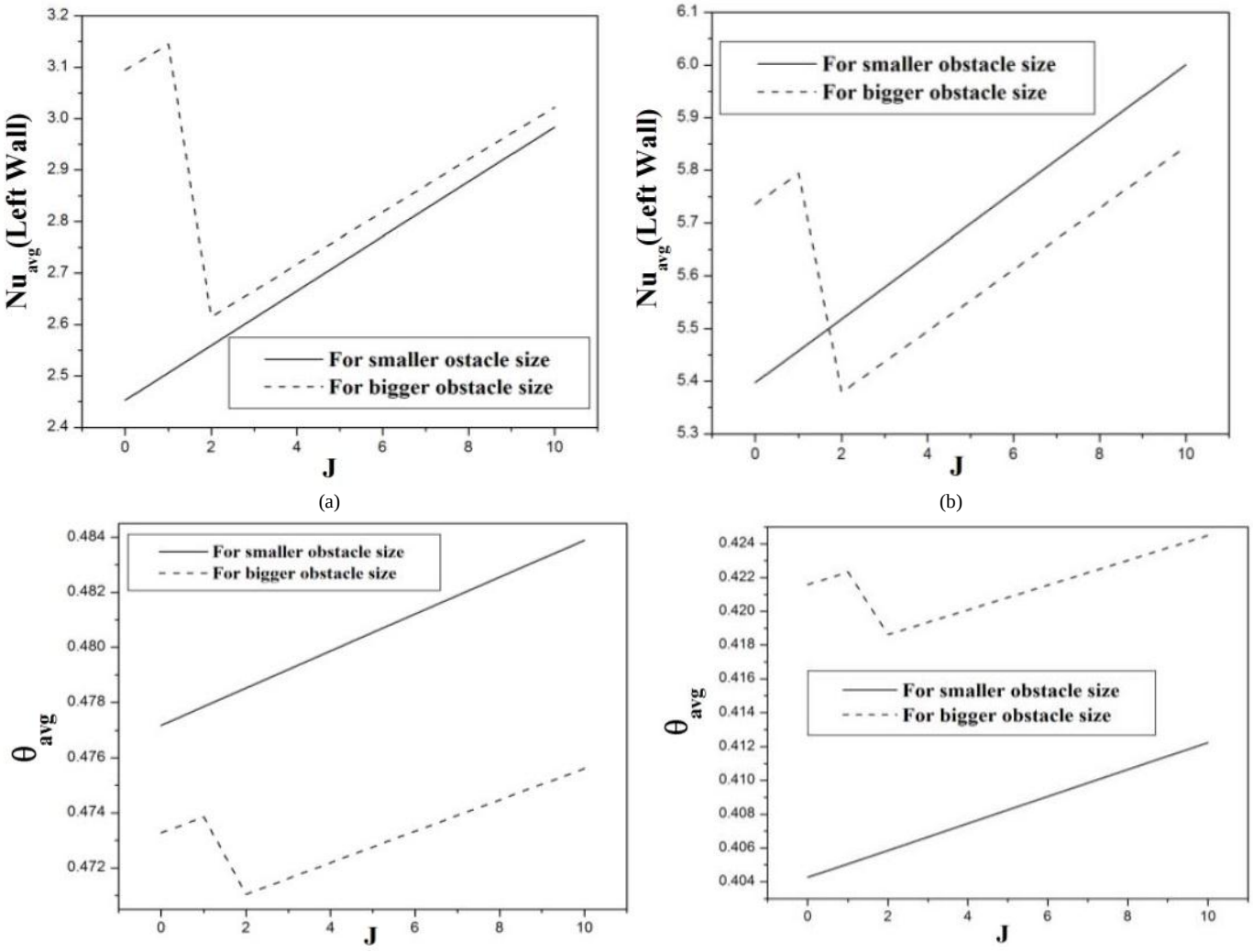

Fig. 8. Variations of average Nusselt Number for both obstacle sizes in case of (a) upward lid motion and (b) downward lid motion; variations of the average fluid temperature for both obstacle sizes in case of (c) upward lid motion and (d) downward lid motion

Also, in case of downward lid motion, the strengths of the streamlines in the immediate vicinity of the obstacle increase with increasing Ri. Further, due to increment in the obstacle dimensions, the corresponding stream function contours retain their overall qualitative appearance but decrease in magnitude in the immediate neighbourhood of the obstacle.The isotherms exhibit higher gradients of temperature with increasing Ri which highlights the dominance of natural convection phenomenon over forced convection and conduction processes for both directions of wall movement. Moreover, an increase in obstacle size causes a subsequent increase in the overall conduction heat transfer process. The average Nusselt Number on the moving left wall depicts an increasing trend for both directions of wall movement. It exhibits higher values for the bigger obstacle size for upward lid motion whereas the trend totally reverses in case of downward lid motion. Also, the Nu values attained for downward lid motion are higher than those for the upward lid motion. Furthermore, the average fluid temperature shows an increasing tendency for both directions of wall movement. However, it shows higher values for smaller obstacle size in case of upward lid motion and bigger obstacle size in case of downward lid motion. Finally, the θavg values for the upward wall movement are higher than those for downward wall motion.

REFERENCES

[1] Prasad A.K. and Koseff J.R. (1996) *Combined forced and natural convection heat transfer in a deep lid-driven cavity flow*, Int. J. Heat and Fluid Flow, 17:460-467.

[2] Chamkha A.J. (2002) *Hydromagnetic combined convection flow in a vertical lid-driven cavity with internal heat generation or absorption*, Numerical Heat Transfer, Part A, 41:529-546.

[3] Cheng T.S. and Liu W.H. (2010) *Effect of temperature gradient orientation on the characteristics of mixed convection flow in a lid-driven square cavity*, Computers & Fluids, 39, 965-978.

[4] Billah M.M., Rahman M.M., Sharif U.M., Rahim N.A., Saidur R., Hasanuzzaman M. (2011) *Numerical analysis of fluid flow due to mixed convection in a lid-driven cavity having a heated circular hollow cylinder*, International Communications in Heat and Mass Transfer, 38, 1093-1103.

[5] Khanafer K. and Aithal S.M. (2013) *Laminar mixed convection flow and heat transfer characteristics in a lid-driven cavity with a circular cylinder*, International Journal of Heat and Mass Transfer, 66, 200-209.

International Journal of Engineering Research & Technology (IJERT)
ISSN: 2278-0181
Vol. 6 Issue 10, October - 2017

[6] Chatterjee D., Halder P., Mondal S., Bhattacharjee S. (2013) *Magnetoconvective Transport in a Vertical Lid-Driven Cavity Including a Heat Conducting Square Cylinder with Joule Heating*, Numerical Heat Transfer, Part A, 64:1050-1071.

[7] Ray S. and Chatterjee D. (2014) *MHD mixed convection in a lid-driven cavity including heat conducting circular solid object and corner heaters with Joule heating*, International Communications in Heat and Mass Transfer, 57, 200-207.

[8] D. Deb, S. Poudel, A. Chakrabarti, "Numerical Simulation of Hydromagnetic Convection in a Lid-driven Cavity Containing a Heat Conducting Elliptical Obstacle with Joule Heating", International Journal of Engineering Research and Technology, Volume. 6 – Issue. 08, August – 2017

[9] Cheng T.S. (2011) *Characteristics of mixed convection heat transfer in a lid-driven square cavity with various Richardson and Prandtl Numbers*, International Journal of Thermal Sciences, 50, 197-205.

[10] Khanafer K. (2014) *Comparison of flow and heat transfer characteristics in a lid-driven cavity between flexible and modified geometry of a heated bottom wall*, International Journal of Heat and Mass Transfer, 78, 1032-1041.

[11] Ismael A.M., Pop I., Chamkha A.J. (2014) *Mixed convection in a lid-driven square cavity with partial slip*, International Journal of Thermal Sciences, 82, 47-61.

[12] Al-Salem K., Öztop H.F., Pop I., Varol Y. (2012) *Effects of moving lid direction on MHD mixed convection in a linearly heated cavity*, International Journal of Heat and Mass Transfer, 55, 1103-1112.

[13] Omari R. (2013) *CFD simulations of lid driven cavity flow at moderate Reynolds Number*, European Scientific Journal, vol.9, No.15.

[14] Davidson P.A., *An Introduction to Magnetohydrodynamics*, Cambridge University Press.

[15] Nag P.K., *Heat and Mass Transfer*, Third Edition, McGraw Hill Education (India) Private Limited, New Delhi.

[16] Schnack D.D., *Lectures in Magnetohydrodynamics With an Appendix on Extended MHD*, Springer.